

Hybrid Open-set Segmentation with Synthetic Negative Data

Matej Grcić, Siniša Šegvić

Abstract—Open-set segmentation is often conceived by complementing closed-set classification with anomaly detection. Existing dense anomaly detectors operate either through generative modelling of regular training data or by discriminating with respect to negative training data. These two approaches optimize different objectives and therefore exhibit different failure modes. Consequently, we propose the first dense hybrid anomaly score that fuses generative and discriminative cues. The proposed score can be efficiently implemented by upgrading any semantic segmentation model with translation-equivariant estimates of data likelihood and dataset posterior. Our design is a remarkably good fit for efficient inference on large images due to negligible computational overhead over the closed-set baseline. The resulting dense hybrid open-set models require negative training images that can be sampled either from an auxiliary negative dataset or from a jointly trained generative model. We evaluate our contributions on benchmarks for dense anomaly detection and open-set segmentation of traffic scenes. The experiments reveal strong open-set performance in spite of negligible computational overhead.

Index Terms—Open-set segmentation, Open-set recognition, Out-of-distribution detection, Anomaly detection, Semantic segmentation, Synthetic data, Normalizing flows

1 INTRODUCTION

HIGH accuracy, fast inference and small memory footprint of modern neural networks [1], [2] steadily expand the horizon of downstream applications. Many exciting applications require advanced image understanding functionality provided by semantic segmentation [3], [4], [5]. These models associate each pixel with a class from a predefined taxonomy [6]. They can accurately segment two megapixel images in real-time on low-power embedded hardware [7], [8], [9]. However, standard training procedures assume closed-world setup, which may raise serious safety issues in real-world deployments [10], [11]. For example, if a segmentation model misclassifies an unknown object (e.g. lost cargo) as road, the autonomous car may experience a serious accident [12]. Such hazards can be alleviated by complementing semantic segmentation with dense anomaly detection [13], [14]. The resulting open-set segmentation models [15] are fitter for real applications due to ability to decline decisions in unknown scene parts.

Previous approaches for open-set segmentation assume either a generative or a discriminative perspective. Generative approaches are based on density estimation [16] or image resynthesis [17], [18], [19]. Discriminative approaches use classification confidence [20], dataset posterior [15] or Bayesian inference [21]. However, the two perspectives exhibit different failure modes. Generative anomaly detectors inaccurately disperse the probability volume [22], [23], [24], [25] or face the hazards of image resynthesis [17], [18]. On the other hand, discriminative anomaly detectors require training on negative content from some general-purpose auxiliary dataset [15], [18], [26]. Such training may involve an overlap between training negatives and test set anomalies.

Hence, the evaluation may lead to over-optimistic performance estimates and surprising failures in production.

In this work, we combine the two perspectives by designing a hybrid anomaly detector. The proposed approach complements a chosen closed-set semantic segmentation model with unnormalized dense dataset likelihood $\hat{p}(\mathbf{x})$ and dense data posterior $P(d_{\text{in}}|\mathbf{x})$. Fusion of these two outputs yields an effective yet efficient dense anomaly detector which we refer to as DenseHybrid. Both components of our anomaly detector require training with negative data [15], [18], [26], [27], [28]. We present a way to relieve that dependence by leveraging synthetic negative data sourced from a generative model [28], [29], [30], [31]. Consequently, our experiments evaluate performance with and without real negative training data.

This paper extends our preliminary conference report [32] by allowing our dense hybrid models to train without real negative data. We achieve that by generating synthetic negative samples with a jointly trained normalizing flow. Different from previous work [31], the normalizing flow does not receive the gradients from the training objectives for anomaly detection. Such design ensures correct convergence of the normalizing flow in view of a complex formulation of the anomaly score, and provides a stronger learning signal to the dataset posterior head. Our new experiments explore open-set performance without training on real negative data and compare our unnormalized density estimator with respect to a general-purpose generative module. Finally, we substantially revise our presentation by supplying a more comprehensive review of the related work and improved descriptions of our method.

Our consolidated work brings forth the following contributions. First, we propose the first hybrid anomaly detector that allows end-to-end training, translational equivariance, and pixel-level predictions. The proposed DenseHybrid

M. Grcić and S. Šegvić are with University of Zagreb, Faculty of Electrical Engineering and Computing, Unska 3, 10000 Zagreb, Croatia
E-mail: {matej.grcic,sinisa.segvic}@fer.hr
Manuscript received January 19, 2023.



Fig. 1. Qualitative performance of the proposed DenseHybrid approach on standard datasets. Top: input images. Bottom: dense maps of the proposed anomaly score. Unknown pixels are assigned with higher anomaly scores designated in yellow. Such a highly accurate anomaly detector enables us to derive the open-set segmentation model.

method combines unnormalized density and discriminative dataset posterior. Both of these two components involve minimal computational overhead and require training on negative data. Second, we extend our approach by allowing it to learn only on inlier images. This configuration leverages synthetic negative data that correspond to generated samples at the boundary of the inlier distribution. Third, we propose open-mIoU as a novel performance metric for open-set segmentation in safety-critical applications. The main strength of the novel metric is exact quantification of the gap between closed-set and open-set setups. Fourth, our DenseHybrid anomaly detector can be easily attached to any closed-set segmentation approach. The resulting open-set segmentation algorithm delivers very competitive performance on standard benchmarks in road-driving scenes with and without training on real negative data.

2 RELATED WORK

The related work considers anomaly detection (Sec. 2.1 and Sec. 2.2), open-set recognition (Sec. 2.3), training open-set recognition on synthetic data (Sec. 2.4), as well as progression towards open-world recognition (Sec. 2.5).

2.1 Image-wide Anomaly Detection

Detecting samples which deviate from the generative process of the training data is a decades old problem [33]. In the machine learning community, this task is also known as anomaly detection, novelty detection and out-of-distribution (OOD) detection [13], [34]. Early image-wide approaches utilize max-softmax probability [34], input perturbations [35] ensembling [36] or Bayesian uncertainty [21]. More encouraging performance has been attained through discriminative training against real negative data [15], [27], [37], [38], adversarial attacks [39] or samples from appropriate generative models [28], [29], [31], [40]. Another line of work detects anomalies by estimating the likelihood. Surprisingly, this research reveals that anomalies may give rise to higher likelihood than inliers [22], [23], [25]. Generative models can mitigate this problem by sharing features with the primary discriminative model [41] and training on negative data [27].

2.2 Pixel-wise Anomaly Detection

Image-wide anomaly detection can be adapted for dense prediction with variable success. Some of the existing image-wide approaches [41] are not applicable in dense prediction context, while others do not perform well [35] or involve excessive computational complexity [35], [36]. On the other hand, concepts such as discriminative training with negative data [27], [37], [42] are easily ported to dense prediction. Hence, several dense anomaly detectors are trained on mixed-content images obtained by pasting negatives (e.g. ImageNet, COCO, ADE20k) over regular training images [15], [18], [26]. Dataset posterior can be recovered by a dedicated head that shares features with the standard semantic segmentation head [15].

Anomalies can also be recognized in feature space [16]. However, this approach complicates detection of small objects due to subsampling and feature collapse [24]. Orthogonally, anomaly detector can be implemented according to learned dissimilarity between the input and the resynthesised image [17], [18], [19], [43]. The resynthesis is performed by a generative model conditioned on the predicted labels. However, this approach is suitable only for uniform backgrounds such as roads [17], and offline applications due to significant computational overhead. Besides dense anomaly detection in road driving scenes, some approaches consider applications in industrial facilities [44]. However, these setups are less relevant for our open-set algorithms since they do not involve the primary discriminative task.

Different than all previous work, we propose the first hybrid anomaly detector for dense prediction models. In comparison with previous approaches that build on dataset posterior [15], [27], [37], our method introduces synergy with likelihood evaluation. In comparison with approaches that recover dense likelihood [10], our method introduces joint hybrid training and efficient joint inference together with standard semantic segmentation. Our method is also related to joint energy-based models [45], since we also reinterpret logits as unnormalized joint likelihood. However, their method has to backprop through the intractable normalization constant and is therefore unsuitable for large resolutions and dense prediction. Our method completely avoids sampling by recovering unnormalized likelihood and training on negative data. Concurrent approaches [46],

[47] consider only the generative component of our hybrid anomaly detector.

2.3 Open-set recognition

Open-set recognition assumes presence of test examples that transcend the training taxonomy. Such examples are also known as semantic anomalies [13]. During inference, the model has to recognize semantic anomalies and withhold (or reject) the decision [48]. The rejection mechanism can be implemented by restricting the shape of the decision boundary [49], [50]. This can be carried out by thresholding the distance from learned class centers in the embedding space [49], [51]. Recognition performance can be further improved through employing a stronger classifier [52], [53]. Alternatively, the rejection mechanism can emerge by complementing the classifier with an anomaly detector [14], [34], [35]. The anomaly detector then detects samples which do not belong to the known classes. We direct the reader to [54] for a comprehensive overview of open-set approaches.

Most open-set approaches quantify performance by separate evaluation of closed-set recognition and anomaly detection [10], [34], [55], [56]. However, such practice does not reveal degradation of discriminative predictions due to errors in anomaly detection [57], [58]. This is especially pertinent to dense prediction models where we can observe inlier and outlier pixels in the same image. Recent work proposes a solution for the related problem of semantic segmentation in adverse conditions [59]. Their uncertainty-aware UIoU metric takes into account prediction confidence as measured by the probability of the winning class. However, UIoU assumes that each pixel belongs to one of the K known classes, which makes it inapplicable for open-set recognition. Different than all previous work, our anomaly-aware open-IOU metric specializes for evaluation of open-set segmentation in presence of outliers. It takes into account both false positive semantic predictions at outliers as well as false negative semantic predictions due to false positive anomaly detection. Furthermore, the difference between mIoU and open-mIoU reveals the performance gap due to presence of outliers in the test set.

2.4 Synthetic data in open-set recognition

Recent seminal approaches train open-set recognition models on synthetic negative data produced by a jointly trained generative adversarial network (GAN) [28], [29]. The GAN is trained to generate inlier data that give rise to low recognition scores for each known class [28]. However, GANs are biased towards limited distribution coverage [24]. Consequently, they are unlikely to span the whole space of possible outliers. Thus, more promising results were achieved by mixing real and synthetic negative samples [40].

Alternatively, GANs can be replaced with generative models that optimize likelihood in order to improve distributional coverage [24]. This task calls for efficient approaches that support fast sampling since joint training requires sample generation on the fly. This puts at disadvantage many interesting generative models such as autoregressive PixelCNN and energy-based models. Normalizing flows are a great candidate for this role due to fast training and capability to quickly generate samples with

different resolutions [31]. Instead of targeting negative data, a generative model can also target negative features [40]. This can be carried out by modelling inlier features and sampling synthetic anomalies from low-likelihood regions of feature space [60]. Negative data have also been crafted by leveraging adversarial perturbations [39].

2.5 Beyond open-set recognition

Anomalous images or pixels can be clustered into new semantic classes. This can be done in incremental [61], [62] or zero/one/few-shot [63] setting. However, these approaches are still unable to compete with supervised learning on standard datasets. We direct reader to [64] for better analysis of pros and cons of low-shot learning.

3 HYBRID SCORE FOR ANOMALY DETECTION

We propose a dense hybrid anomaly score that improves upon discriminative and generative anomaly detection (Sec. 3.1). The new hybrid anomaly score can be efficiently fused with a semantic classifier (Sec. 3.2).

We represent the input images with a random variable $\underline{\mathbf{x}}$. Variable \underline{y}^{ij} denotes the corresponding label at the location (i, j) , while binary random variable \underline{d}^{ij} models whether a given pixel belongs to the inliers or outliers. We write \underline{d}_{in}^{ij} for inliers and \underline{d}_{out}^{ij} for outliers. We denote a realization of a random variable without the underline. Thus, $P(y^{ij}|\underline{\mathbf{x}})$ is a shortcut for $P(\underline{y}^{ij} = y^{ij}|\underline{\mathbf{x}} = \mathbf{x})$. For brevity, we often omit spatial locations.

3.1 Hybrid Anomaly Detection for Dense Prediction

Generative and discriminative approaches to anomaly detection exhibit different failure modes. Fig. 2 illustrates the shortcomings of both approaches on a toy problem. Blue dots designate inlier data. Green triangles designate the negative data used for training. Red squares denote anomalous test data. Discriminative detectors model dataset posterior $P(d_{out}|\underline{\mathbf{x}})$. They fail if the negative training data does not cover the entire negative manifold (left) [27]. On the other hand, generative detectors which model $p(\underline{\mathbf{x}})$ tend to inaccurately distribute probability volume over the sample space [22], [23], [24] (center). We fuse discriminative and generative approaches into a hybrid detector that alleviates the aforementioned limitations (right).

We build our hybrid anomaly detector upon the discriminative dataset posterior $P(d_{in}|\underline{\mathbf{x}})$ and the generative data likelihood $p(\underline{\mathbf{x}})$. We express a novel hybrid anomaly score as log-ratio between $P(d_{out}|\underline{\mathbf{x}}) = 1 - P(d_{in}|\underline{\mathbf{x}})$ and $p(\underline{\mathbf{x}})$:

$$s(\underline{\mathbf{x}}) := \ln \frac{P(d_{out}|\underline{\mathbf{x}})}{p(\underline{\mathbf{x}})} = \ln P(d_{out}|\underline{\mathbf{x}}) - \ln p(\underline{\mathbf{x}}). \quad (1)$$

We will further show that this formulation is especially suitable for dense predictions atop the dense classifier. There may be other effective formulations of $s(\underline{\mathbf{x}})$, which is an interesting direction for future work.

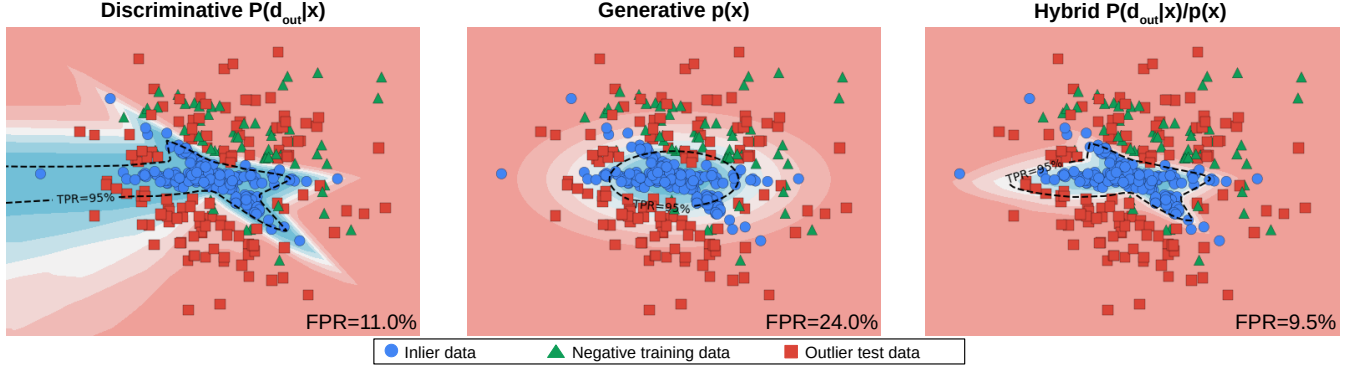


Fig. 2. Anomaly detection on a toy dataset. The discriminative approach (left) models the dataset posterior. It fails if the negative training dataset fails to cover all modes of the test anomalies. The generative approach (middle) models the data likelihood. It may assign high likelihoods to test anomalies [22] due to over-generalization [24]. The hybrid approach attains a synergy between discriminative and generative modelling.

3.2 Efficient Implementation Atop Semantic Classifier

Standard semantic classification can be viewed as a two-step procedure. Given an input image \mathbf{x} , a deep feature extractor f_{θ_1} computes an abstract representation \mathbf{z} also known as pre-logits. The computed pre-logits are projected into logits \mathbf{s} , and activated by softmax. The softmax output is defined as class posterior probability $P(y|\mathbf{x})$:

$$P(y|\mathbf{x}) := \text{softmax}(\mathbf{s})_y, \text{ where } \mathbf{s} = f_{\theta_2}(\mathbf{z}), \mathbf{z} = f_{\theta_1}(\mathbf{x}). \quad (2)$$

In practice, f_{θ_1} is an encoder-decoder architecture common for semantic segmentation and f_{θ_2} is a simple projection by means of 1x1 convolution. We extend this framework with dense data likelihood and discriminative dataset posterior.

Dense data likelihood can be conveniently derived atop dense classifier by re-interpreting logits as unnormalized joint probability of input and label [45]:

$$p(y, \mathbf{x}) = \frac{1}{Z} \hat{p}(y, \mathbf{x}) := \frac{1}{Z} \exp \mathbf{s}_y, \text{ where } \mathbf{s} = f_{\theta_2}(\mathbf{z}). \quad (3)$$

Z denotes the corresponding normalization constant dependent only on model parameters. As usual, Z is finite but intractable, since it requires computing the unnormalized distribution for all realizations of \underline{y} and $\underline{\mathbf{x}}$: $Z = \sum_{\mathbf{x}} \sum_y \exp \mathbf{s}_y$. Throughout this work, we conveniently eschew the evaluation of Z in order to enable efficient training and inference.

We express the dense likelihood $p(\mathbf{x})$ by marginalizing out \underline{y} :

$$p(\mathbf{x}) = \sum_y p(y, \mathbf{x}) = \frac{1}{Z} \sum_y \hat{p}(y, \mathbf{x}) = \frac{1}{Z} \sum_y \exp \mathbf{s}_y. \quad (4)$$

Standard discriminative predictions are easily recovered through Bayes rule $p(y, \mathbf{x})/p(\mathbf{x})$:

$$P(y|\mathbf{x}) = \frac{p(y, \mathbf{x})}{\sum_{y'} p(y', \mathbf{x})} = \frac{\exp \mathbf{s}_y}{\sum_{y'} \exp \mathbf{s}_{y'}} = \text{softmax}(\mathbf{s})_y. \quad (5)$$

The normalization constant Z appears both in the numerator and denominator, and hence can be cancelled out. Reinterpretation of logits as unnormalized joint probability enables likelihood estimation atop a discriminative classifier task and even exploiting pretrained classifiers. Note that adding a constant value to the logits does not affect the standard classification but affects our framework since the value of $p(\mathbf{x})$ changes. Hence, we use the extra degree of

freedom in logits to express the data likelihood [45]. The same extra degree of freedom has been used to model a discriminator network in semi-supervised learning [65].

We define the dataset posterior $P(d_{\text{in}}|\mathbf{x})$ as a non-linear transformation based on pre-logits \mathbf{z} [15]:

$$P(d_{\text{in}}|\mathbf{x}) := \sigma(g_{\gamma}(\mathbf{z})). \quad (6)$$

In our case, the function g is BN-ReLU-Conv1x1 of pre-logits, followed by a sigmoid non-linearity.

We can now compute the proposed dense hybrid anomaly score (1) atop the classifier as:

$$s(\mathbf{x}) := \ln P(d_{\text{out}}|\mathbf{x}) - \ln \hat{p}(\mathbf{x}) + \ln Z \quad (7)$$

$$\cong \ln P(d_{\text{out}}|\mathbf{x}) - \ln \hat{p}(\mathbf{x}). \quad (8)$$

We can neglect Z since ranking performance [34] is invariant to monotonic transformations such as taking a logarithm or adding a constant. Note that the logarithmic function re-scales the unnormalized $\hat{p}(\mathbf{x})$ and $P(d_{\text{out}}|\mathbf{x})$ on approximately the same scale, equalizing the influence of both components in the final decision. The resulting formulation (7) is especially well suited for dense prediction due to minimal overhead and translation equivariance.

Figure 3 illustrates dense inference with the proposed hybrid open-set setup. RGB input is fed to a hybrid dense model which produces pre-logit activations \mathbf{z} and logits \mathbf{s} . We activate the closed-set class posterior $P(y|\mathbf{x})$ with softmax and the unnormalized data log-likelihood $\ln \hat{p}(\mathbf{x})$ via log-sum-exp operator (designated in green). A distinct head g transforms pre-logits \mathbf{z} into the dataset posterior $P(d_{\text{out}}|\mathbf{x})$ (designated in yellow). The anomaly score $s(\mathbf{x})$ is a log ratio between the latter two outputs. The resulting anomaly map is thresholded and fused with the discriminative output into the final dense open-set recognition map.

4 OPEN-SET TRAINING WITH DENSEHYBRID

Our open-set approach complements an arbitrary closed-set segmentation model with the DenseHybrid anomaly detector. We propose a novel training setup that eschews the intractable normalization constant by introducing negative data to the generative learning objective (Sec. 4.1). The same negative data are used to train the dataset posterior. We relax dependence on real negatives by sampling a suitably trained normalizing flow (Sec. 4.2).

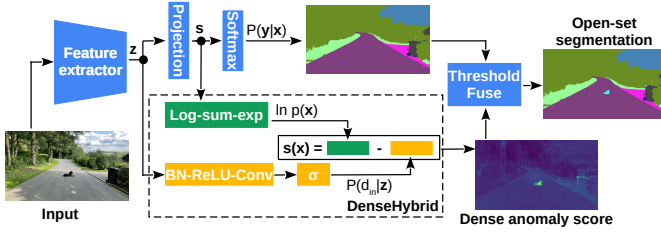


Fig. 3. The proposed open-set segmentation approach. Our anomaly score is the log-ratio of dense data likelihood and discriminative dataset posterior. Both outputs are derived from the standard dense classifier. We formulate open-set segmentation by complementing the closed-set segmentation map with the thresholded anomaly score.

4.1 Open-set training with real negative data

The multi-task model from Fig. 3 requires joint fine-tuning of three dense prediction heads: i) closed-set class posterior $P(y|\mathbf{x})$, ii) unnormalized data likelihood $\hat{p}(\mathbf{x})$ [45], and iii) dataset posterior $P(d_{\text{in}}|\mathbf{x})$ [15]. The class-posterior head requires a discriminative loss over the inlier dataset D_{in} :

$$L_{\text{cls}}(\theta) = \mathbb{E}_{\mathbf{x}, y \in D_{\text{in}}} [-\ln P(y|\mathbf{x})] \quad (9)$$

$$= -\mathbb{E}_{\mathbf{x}, y \in D_{\text{in}}} [\mathbf{s}_y - \ln \sum_{y'} \exp \mathbf{s}_{y'}]. \quad (10)$$

Training unnormalized likelihood is a daunting task since backpropagation through $p(\mathbf{x})$ involves intractable integration over all possible images [66], [67]. Previous solutions are based on MCMC sampling [45], however, this is not feasible in our setup due to high-resolution inputs and dense prediction. We eschew the normalization constant by optimizing the likelihood both in inlier and outlier pixels:

$$L_{\mathbf{x}}(\theta) = \mathbb{E}_{\mathbf{x} \in D_{\text{in}}} [-\ln p(\mathbf{x})] - \mathbb{E}_{\mathbf{x} \in D_{\text{out}}} [-\ln p(\mathbf{x})] \quad (11)$$

$$= -\mathbb{E}_{\mathbf{x} \in D_{\text{in}}} [\ln \hat{p}(\mathbf{x})] - \ln Z + \mathbb{E}_{\mathbf{x} \in D_{\text{out}}} [\ln \hat{p}(\mathbf{x})] + \ln Z \quad (12)$$

$$= -\mathbb{E}_{D_{\text{in}}} \left[\ln \sum_i \exp(\mathbf{s}_i) \right] + \mathbb{E}_{D_{\text{out}}} \left[\ln \sum_i \exp(\mathbf{s}_i) \right] \quad (13)$$

As before, \mathbf{s} stands for logits computed by f_{θ} . Note that the normalization constant Z cancels out due to training on outliers. In practice, we use a simplified loss that corresponds to an upper bound of the above expression ($L_{\mathbf{x}}^{\text{UB}} \geq L_{\mathbf{x}}$):

$$L_{\mathbf{x}}^{\text{UB}}(\theta) = -\mathbb{E}_{\mathbf{x}, y \in D_{\text{in}}} [\mathbf{s}_y] + \mathbb{E}_{\mathbf{x} \in D_{\text{out}}} \left[\ln \sum_i \exp(\mathbf{s}_i) \right]. \quad (14)$$

Proof can be easily derived by recalling that log-sum-exp is a smooth upper bound of the max function. Thus, our upper bound $L_{\mathbf{x}}^{\text{UB}}$ leverages the following inequalities:

$$\ln \sum_i \exp \mathbf{s}_i \geq \max_i \mathbf{s}_i \geq \mathbf{s}_y. \quad (15)$$

Comparison of the discriminative loss (9) and the generative upper bound (14) reveals that the standard classification loss is well aligned with the upper bound in inlier pixels. Recall that training data likelihood only on inliers [45], [66] would require MCMC sampling, which is infeasible in our context. Unnormalized likelihood could also be trained through score matching [67]. However, this would preclude hybrid modelling due to having to train

on noisy inputs. Consequently, it appears that the proposed training approach is a method of choice in our context.

The dataset-posterior head $P(d_{\text{in}}|\mathbf{x})$ requires a discriminative loss that distinguishes the inlier dataset D_{in} from the outlier dataset D_{out} [15]:

$$L_{\text{d}}(\theta, \gamma) = -\mathbb{E}_{\mathbf{x} \in D_{\text{in}}} [\ln P(d_{\text{in}}|\mathbf{x})] - \mathbb{E}_{\mathbf{x} \in D_{\text{out}}} [\ln(1 - P(d_{\text{in}}|\mathbf{x}))]. \quad (16)$$

Our final compound loss aggregates L_{cls} , $L_{\mathbf{x}}^{\text{UB}}$ and L_{d} :

$$L(\theta, \gamma) = -\mathbb{E}_{\mathbf{x}, y \in D_{\text{in}}} [\ln P(y|\mathbf{x}) + \ln P(d_{\text{in}}|\mathbf{x})] - \beta \cdot \mathbb{E}_{\mathbf{x} \in D_{\text{out}}} [\ln(1 - P(d_{\text{in}}|\mathbf{x})) - \ln \hat{p}(\mathbf{x})]. \quad (17)$$

Hyperparameter β controls the impact of negative data to the primary classification task. Note that we omit the first term from $L_{\mathbf{x}}^{\text{UB}}$ (14) in inlier pixels since this is implicitly enforced through optimization of L_{cls} (9).

Figure 4 illustrates the described procedure for training open-set segmentation models. We prepare mixed-content training images x' by pasting negative patches x^- into regular training images x^+ :

$$\mathbf{x}' = (1 - \mathbf{s}) \cdot \mathbf{x}^+ + \text{pad}(\mathbf{x}^-, \mathbf{m}), \quad \mathbf{x}^- \in D_{\text{out}}. \quad (18)$$

Note that here we leverage real negative images $x^- \in D_{\text{out}}$. We consider synthetic negatives in the subsequent subsection. The binary mask \mathbf{m} identifies negative pixels within the mixed-content image x' . Negative pixels are labelled as d_{out} while positive pixels are labelled as d_{in} . Semantic labels of negative pixels are set to void.

The resulting mixed-content image x' is fed to the desired semantic segmentation model that produces pre-logits \mathbf{z} and logits \mathbf{s} . We recover the class posterior $P(y|\mathbf{x})$ by activating logits with softmax. We recover the unnormalized log-likelihood $\ln \hat{p}(\mathbf{x})$ by processing logits with log-sum-exp. We recover dataset posterior $P(d_{\text{in}}|\mathbf{x})$ by processing pre-logit activations with the standard BN-ReLU-Conv1 \times 1 unit. The compound training loss $L(\theta, \gamma)$ (17) aggregates class-discriminative loss L_{cls} (9), generative loss $L_{\mathbf{x}}^{\text{UB}}$ (14) and dataset-discriminative loss L_{d} (16).

4.2 Open-set training with synthetic negative data

Anomaly detectors can avoid biased predictions by replacing real negative training data with samples of a suitable generative model [28], [30], [31], [68]. The generative model has to be trained to generate synthetic samples that encompass the border of the inlier distribution [28]. The required learning signal can be derived from discriminative predictions [28], [30], [31] or provided by an adversarial module [39]. Hence, replacing real negative data with synthetic counterparts requires joint training of the generative model. We choose a normalizing flow [69] for this task due to exceptional distributional coverage and ability to quickly generate samples of varying spatial dimensions [70]. We train the normalizing flow p_{ζ} according to a weighted sum of two loss terms: L_{mle} and L_{jsd} .

The data term L_{mle} corresponds to negative log-likelihood of random crops from inlier images x^+ :

$$L_{\text{mle}}(\zeta) = -\mathbb{E}_{\mathbf{x}^+ \in D_{\text{in}}} [\ln p_{\zeta}(\text{crop}(\mathbf{x}^+))]. \quad (19)$$

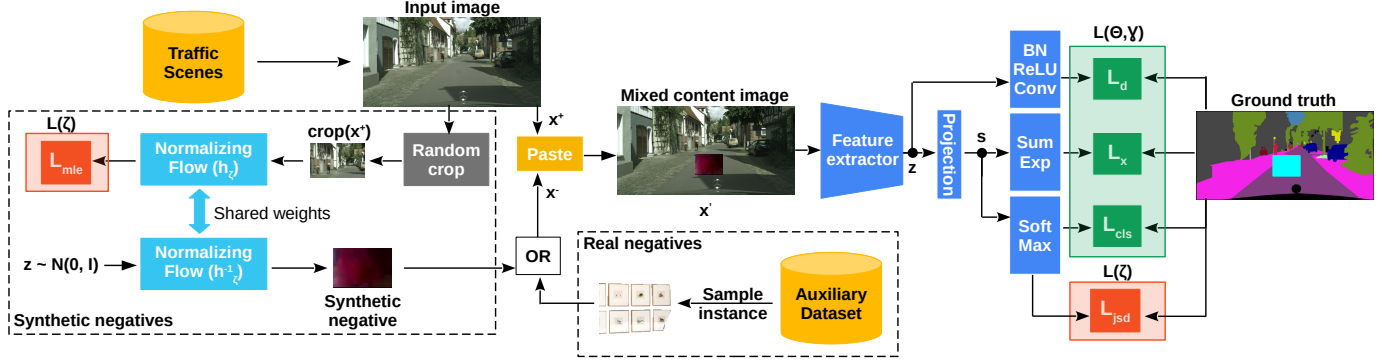


Fig. 4. The two training procedures for the proposed open-set training with DenseHybrid. We construct mixed-content images by pasting negatives into inlier images. The negative training data can be sampled either from an auxiliary real dataset (Sec. 4.1) or from a jointly trained normalizing flow (Sec. 4.2). Mixed-content images are fed to the open-set model with three dense outputs: closed-set class posterior, unnormalized likelihood, and dataset posterior. Outputs are optimized according to the compound loss (17). In the case of synthetic negatives, the normalizing flow optimizes the loss (20).

The crop notation mirrors the pad notation from (18). Random crops vary in spatial resolution. This term aligns the generative distribution with the distribution of the training data. It encourages coverage of the entire inlier distribution under the condition that the generative model has sufficient capacity.

The boundary-attraction term L_{jsd} [70] corresponds to negative Jensen-Shannon divergence between the class-posterior and the uniform distribution at all generated pixels. This term pushes the generative distribution towards the periphery of the inlier distribution where the class posterior should be unclear. Note that gradients of this term must propagate through the entire semantic model in order to reach the normalizing flow. Hence, the flow is penalized when the generated sample yields high softmax confidence. This signal pushes the generative distribution away from high-density regions of the input space [28].

The total loss of the normalizing flow modulates the contribution of the boundary term with the hyperparameter λ :

$$L(\zeta) = L_{mle}(\zeta) + \lambda \cdot L_{jsd}(\zeta; \theta) \quad (20)$$

Optimization of this loss enforces the generative distribution to encompass all modes of inlier distribution. Note that our normalizing flow can never match the diversity of images from a real dataset such as COCO or ADE20k. It would be unreasonable to expect a generative model to draw a sofa after training on Cityscapes. Still, if the flow succeeded to learn well the boundary of the inlier distribution, then DenseHybrid would be inclined to recognize all off-distribution samples as anomalies [28].

Details of the training procedure are again illustrated in Figure 4. We sample the normalizing flow by i) selecting a random spatial resolution (H, W) from a predefined interval, ii) sampling a random latent representation $z \sim \mathcal{N}(0, I_{HW})$, and iii) feeding z to the flow so that $x^- = h_\zeta^{-1}(z)$. We again craft a mixed-content image x' by pasting the synthesized negative patch x^- into the regular training image x^+ according to (18). We perform the forward pass, determine L_{cls} , L_d , L_x , and L_{jsd} , and recover the training gradients by backpropagation. Of course, gradient of L_{jsd} is propagated all the way to the normalizing flow. We now take the deleted

inlier patch x_s^+ , perform inference with the normalizing flow ($z = h_\zeta(x_s^+)$) and accumulate gradients of L_{mle} before performing a model-wide parameter update.

5 EXPERIMENTAL SETUP

We describe benchmarks and datasets used for the evaluation of DenseHybrid in dense anomaly detection and open-set segmentation experiments (Sec. 5.1). We propose a new metric to adequately quantify the gap between the open-set and closed-set performance (Sec. 5.2). Also, we present the main implementation details of our solution (Sec. 5.3).

5.1 Benchmarks and Datasets

We evaluate performance on standard benchmarks for dense anomaly detection and open-set segmentation. Fishyscapes [10] considers urban scenarios on a subset of LostAndFound [12] and on Cityscapes validation images with pasted anomalies (FS Static). SegmentMeIfYouCan (SMIYC) [56] collects carefully selected images from the real world and groups them with respect to the anomaly size into AnomalyTrack (large) and ObstacleTrack (small). Moreover, the benchmark includes a selection of images of the LostAndFound dataset [12] in which the lost objects do not correspond to the Cityscapes taxonomy. Unfortunately, both benchmarks supply only binary labels, which makes them inappropriate for evaluating open-set performance. Hence, we report only anomaly detection performance on these benchmarks. We also validate performance on Cityscapes while reinterpreting a subset of ignore classes as the unknown class [40].

StreetHazards [71] is a synthetic dataset created with CARLA virtual environment. The simulated environment enables smooth anomaly injection and low-cost label extraction. Consequently, the dataset contains $K+1$ labels, making it suitable for measuring open-set recognition performance.

5.2 Measuring open-set performance

Previous work evaluates open-set segmentation through anomaly detection [12], [56] and closed-set segmentation

[10]. The reported drop in closed-set performance is usually negligible and is explained by the allocation of model capacity for anomaly detection. However, we will show that the impact of anomalies onto segmentation performance can be clearly characterized only in the open-set setup. More precisely, we shall take into account false positive semantic predictions at anomalies as well as false negative semantic predictions due to false anomaly detections.

We propose a novel evaluation procedure for open-set segmentation. Our procedure starts by thresholding the anomaly score so that it yields 95% TPR anomaly detection on held-out data. This is equivalent to the 5th percentile of inlier scores. Then, we override the classification in pixels which score higher than the threshold. This yields a recognition map with $K+1$ labels. We assess open-set segmentation performance according to a novel metric that we term open-mIoU. We compute open-IoU for the k -th class as follows:

$$\text{open-IoU}_k = \frac{TP_k}{TP_k + FP_k^{\text{os}} + FN_k^{\text{os}}}, \quad \text{where} \quad (21)$$

$$FP_k^{\text{os}} = \sum_{i=1, i \neq k}^{K+1} FP_k^i, \quad FN_k^{\text{os}} = \sum_{i=1, i \neq k}^{K+1} FN_k^i. \quad (22)$$

Different that the standard IoU formulation, open-IoU takes into account false positives and false negatives caused by applying imperfect anomaly detectors at open-set pixels. In particular, a prediction of class k at an outlier pixel (false negative anomaly detection) counts as a false positive for class k . Furthermore, a prediction of class $K+1$ at a pixel labelled as class k (false positive anomaly detection) counts as a false negative for class k . Note that we still average open-IoU over K inlier classes. Thus, a recognition model with perfect anomaly detection gets assigned the same performance as in the closed world. Note that this property would not be preserved if we averaged open-IoU over $K+1$ classes. Hence, a comparison between closed-set mIoU and open-set open-mIoU quantifies the gap between the open and closed-set performance. Some experiments report F_1 score averaged over $K+1$ classes [40], [57]. However, mF_1 can not be used to quantify the performance gap.

Figure 5 compares the closed-set (left) and open-set (right) evaluation protocols. Imperfect anomaly detection impacts recognition performance through increased false positive semantics (designated in yellow) and false negative semantics (designated in red). The difference between closed-set mIoU and open-mIoU reveals the performance drop due to inaccurate anomaly detection.

Measuring performance according to open-mIoU requires datasets with $K+1$ labels. Collecting and annotating a dataset with such taxonomy requires substantial resources. Currently, only StreetHazards [71] offers this opportunity.

5.3 Implementation Details

The proposed approach can be easily applied to any pre-trained semantic segmentation baseline: the only requirement is access to pre-logit features and dense logits. We append an additional branch g_γ which is in our case BN-ReLU-Conv1x1, to compute the discriminative dataset posterior. We obtain unnormalized likelihood as the sum

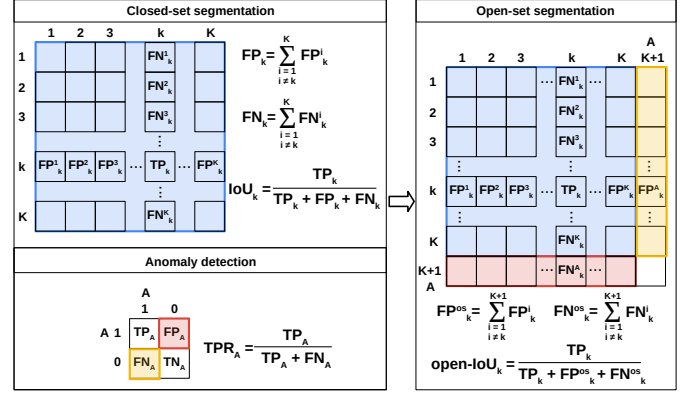


Fig. 5. We extend closed-set performance evaluation (left) with a novel open-set metric (right). Open-IoU takes into account false positive semantics at anomalies as well as false negative semantics due to false anomaly detections. The proposed open-mIoU metric quantifies recognition performance in presence of anomalies.

of exponentiated logits. We fine-tune the resulting open-set models on mixed-content images with pasted negative ADE20k instances (4.1) or synthetic negative patches (4.2).

In the case of SMIYC, we fine-tune LDN-121 [75] for 10 epochs on images from Cityscapes [76], Vistas [77] and Wild-dash2 [55]. In the case of Fishyscapes, we use DeepLabV3+ with WideResNet38 [78]. We fine-tune the model for 10 epochs on Cityscapes. In the case of StreetHazards, we train LDN-121 for 120 epochs in the closed-world setting and then fine-tune the open-set model on mixed-content images.

Configurations that do not rely on real negative data leverage synthetic data of varying resolution as generated by DenseFlow-45-6 [69]. All such experiments pre-train DenseFlow with the standard MLE loss on 64×64 crops from road-driving images prior to joint learning. Our fine-tuning experiments last less than 24h on RTX A5000 GPU. Our source code is publicly available [79].

6 EXPERIMENTAL RESULTS

We evaluate DenseHybrid performance in dense anomaly detection (Sec. 6.1) and open-set segmentation (Sec. 6.2) experiments, after training with and without real negative data. We also ablate the design choices (Sec. 6.3), explore the influence of distance (Sec. 6.4), and present the computational requirements of the proposed module (Sec. 6.5).

6.1 Dense Anomaly Detection in Open-set Setups

Table 1 presents dense anomaly detection performance on SMIYC [56] and Fishyscapes [16]. We include our model trained on real negative data (DenseHybrid) as well as our model trained on synthetic negatives (SynDenseHybrid). DenseHybrid outperforms contemporary approaches on both AnomalyTrack and ObstacleTrack by a wide margin. Also, it achieves the best FPR_{95} on LostAndFound-noKnown. Similarly, it delivers the best performance on Fishyscapes LostAndFound and the best FPR_{95} on Static.

DenseHybridSyn outperforms all previous methods that do not train on real negative data on ObstacleTrack and LostAndFound-noKnown. In the case of AnomalyTrack, it is outperformed only by image resynthesis [17] that requires

TABLE 1

Anomaly detection performance on SegmentMelfYouCan [56] and Fishyscapes [16]. Aux data denotes training on real negatives, while Img rsyn. denotes image resynthesis.

Method	Aux data	Img rsyn.	SegmentMelfYouCan [56]				Fishyscapes [10]				CS val IoU		
			AnomalyTrack		ObstacleTrack		LAF-noKnown		FS LAF			FS Static	
			AP	FPR ₉₅	AP	FPR ₉₅	AP	FPR ₉₅	AP	FPR ₉₅	AP	FPR ₉₅	
Image Resyn. [17]	X	✓	52.3	25.9	37.7	4.7	57.1	8.8	5.7	48.1	29.6	27.1	81.4
Road Inpaint. [72]	X	✓	-	-	54.1	47.1	82.9	35.8	-	-	-	-	-
Max softmax [34]	X	X	28.0	72.1	15.7	16.6	30.1	33.2	1.8	44.9	12.9	39.8	80.3
MC Dropout [21]	X	X	28.9	69.5	4.9	50.3	36.8	35.6	-	-	-	-	-
ODIN [35]	X	X	33.1	71.7	22.1	15.3	52.9	30.0	-	-	-	-	-
SML [73]	X	X	-	-	-	-	-	-	31.7	21.9	52.1	20.5	-
Embed. Dens. [10]	X	X	37.5	70.8	0.8	46.4	61.7	10.4	4.3	47.2	62.1	17.4	80.3
JSRNet [19]	X	X	33.6	43.9	28.1	28.9	74.2	6.6	-	-	-	-	-
SynDenseHybrid (ours)	X	X	51.5	33.2	64.0	0.6	78.8	1.1	51.8	11.5	54.7	15.5	79.9
SynBoost [18]	✓	✓	56.4	61.9	71.3	3.2	81.7	4.6	43.2	15.8	72.6	18.8	81.4
Prior Entropy [74]	✓	X	-	-	-	-	-	-	34.3	47.4	31.3	84.6	70.5
OOD Head [42]	✓	X	-	-	-	-	-	-	31.3	19.0	96.8	0.3	79.6
Void Classifier [10]	✓	X	36.6	63.5	10.4	41.5	4.8	47.0	10.3	22.1	45.0	19.4	70.4
Dirichlet prior [74]	✓	X	-	-	-	-	-	-	34.3	47.4	84.6	30.0	70.5
DenseHybrid (ours)	✓	X	78.0	9.8	87.1	0.2	78.7	2.1	43.9	6.2	72.3	5.5	81.0

significant computational overhead. Also, DenseHybridSyn achieves the best performance on all but one metric of Fishyscapes and the second-best AP on Fishyscapes Static. As in the case of training on real negative data, the hybrid anomaly detector achieves the best performance on Fishyscapes with exception of AP on Static. Note that the presented performance evaluation uses standard performance metrics of the particular datasets. Our performance metrics on Fishyscapes LostAndFound would increase if we considered only the road pixels as in [19]. The rightmost column of the table indicates that our fine-tuning protocol exerts a negligible impact on closed-set performance. However, the next section will show that the impact of anomaly detection on final recognition performance is more significant than what can be measured with closed-set metrics.

Figure 6 shows synthetic negatives produced by the training setup from Sec. 4.2. Samples vary in spatial resolution and lack meaningful visual concepts. Yet, training our open-set model on such samples yields only slightly worse performance than when training on real negative data.

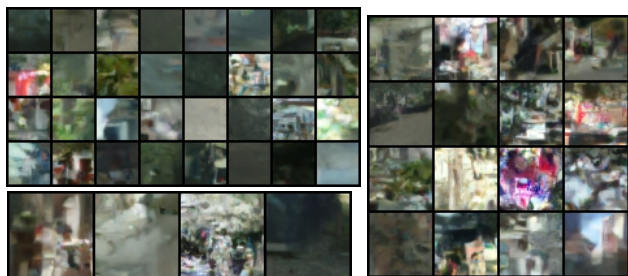


Fig. 6. Synthetic negatives produced by a normalizing flow trained as described in Sec. 4.2. These samples are pasted into training crops instead of real negative images (instances from ADE20k). We sample the normalizing flow at different resolutions in order to mimic real-world anomalies which vary in size.

Table 2 presents performance on Road Anomaly [17] and on validation subsets of Fishyscapes. The top section presents methods which do not train on real negative data. The bottom section presents methods which train on real

negative data. Our method performs competitively with respect to the previous works in both setups.

TABLE 2

Performance of DenseHybrid on Road Anomaly and Fishyscapes val. DenseHybrid delivers strong performance when trained with and without real negative images.

Model	RA		FS L&F		FS Static	
	AP	FPR	AP	FPR	AP	FPR
MSP [34]	15.7	71.4	4.6	40.6	19.1	24.0
ML [71]	19.0	70.5	14.6	42.2	38.6	18.3
SML [73]	25.8	49.7	36.6	14.5	48.7	16.8
SynthCP [43]	24.9	64.7	6.5	46.0	23.2	34.0
Density [10]	-	-	4.1	22.3	-	-
SynDenseHybrid	35.1	37.2	59.5	10.4	49.0	10.3
SynBoost [18]	38.2	64.8	60.6	31.0	66.4	25.6
OOD head [15]	-	-	45.7	24.0	-	-
Energy [38]	19.5	70.2	16.1	41.8	41.7	17.8
DenseHybrid	63.9	43.2	60.5	6.0	63.1	4.2

We validate our method by considering a subset of Cityscapes void classes as the unknown class [40]. More precisely, we consider all void classes except ‘unlabeled’, ‘ego vehicle’, ‘rectification border’, ‘out of roi’ and ‘license plate’ as unknowns during validation. Table 3 compares performance according to the AUROC (AUC) metric. SynDenseHybrid outperforms all previous works. Most notably, it outperforms the previous state of the art [40] by three percentage points. To offer fair comparison with previous work, we do not report results when training on real negative data since such data was not used in related work [40], [80].

TABLE 3

Open-set segmentation performance on Cityscapes val. Following [40], we consider a subset of ignored classes as unknowns.

Method	AUC	Method	AUC
MSP [34]	72.1	GDM [81]	74.3
Entropy [82]	69.7	GMM [68]	76.5
OpenMax [50]	75.1	K+1 classifier	75.5
C2AE [80]	72.7	OpenGAN-O [40]	70.9
ODIN [35]	75.5	OpenGAN [40]	88.5
MC dropout [21]	76.7	SynDenseHybrid (ours)	91.7

6.2 Open-set Segmentation

We recover open-set segmentation by fusing a closed-set segmentation with properly thresholded dense anomaly detection (Fig. 3). Such model detects anomalous regions, while also correctly classifying inlier parts of the scene. We measure open-set performance on the StreetHazards dataset according to mean F_1 (\overline{F}_1) score and the proposed open-mIoU (\overline{oIoU}) metric. We partition the test subset into two folds which correspond to the two test cities - t5 and t6. We set the anomaly score threshold in order to obtain 95% TPR on t5, and measure open-mIoU on t6. Subsequently, we switch the folds and measure open-mIoU on t5. We compute the overall open-mIoU by weighting these two measurements according to the number of images in the two folds. Table 4 presents performance evaluation on StreetHazards. The left part of the table considers anomaly detection while the right part of the table considers closed-set and open-set segmentation performance. Our method outperforms contemporary approaches in anomaly detection both with and without training on real negative data. Furthermore, our method achieves the best open-set performance (columns \overline{oIoU} and \overline{F}_1) despite lower closed-set segmentation score (\overline{IoU} column). The performance drop between closed-set and open-set can be quantified as the difference between \overline{IoU} and \overline{oIoU} ("Gap" column). Our method achieves the least performance gap of around 18 percentage points. Nevertheless, an ideal anomaly detector would achieve equal open-set and closed-set metrics. Hence, we conclude that even the state-of-the-art anomaly detectors are still insufficient for delivering closed-set performance in open-set setups. Researchers should strive to further close this gap in order to improve the safety of recognition systems in the real world. We implemented [38], [84] into

also reports performance on StreetHazards, however, they aim to detect classification errors instead of anomalies.

Figure 7 visualises qualitative open-set segmentation performance on StreetHazards test. Our hybrid anomaly detector accurately combines dense anomaly detection (second row) with closed-set segmentation and delivers open-set segmentation (third row). We also show the energy-based approach [38] which yields more false positives (fourth row).

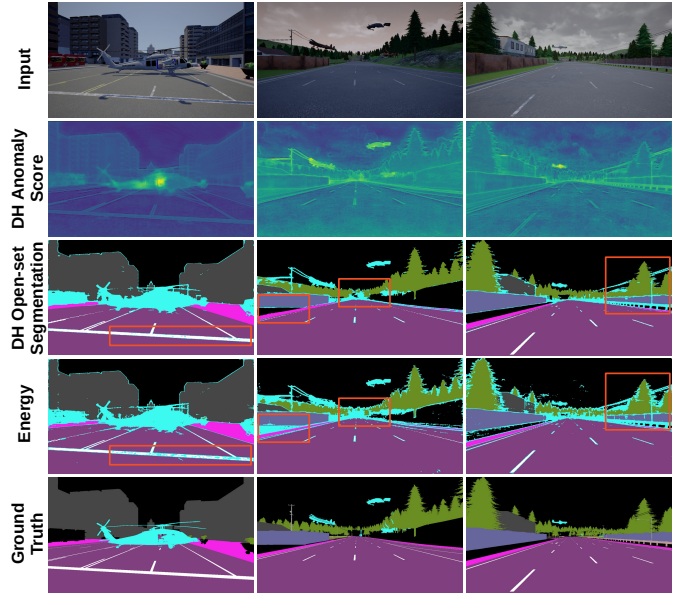


Fig. 7. Qualitative open-set segmentation performance on StreetHazards. DenseHybrid (rows 2 and 3) has more accurate open-set performance compared to the energy-based approach [38](row 4), as denoted with red rectangles. Zoom in for a better view.

TABLE 4

Performance evaluation on StreetHazards [71]. We evaluate anomaly detection (Anomaly), closed-set segmentation (Cls.), open-set segmentation (Open-set), and the open-set gap (Gap). Our DenseHybrid delivers competitive open-set performance.

Method	Anomaly			Cls.	Open-set		Gap
	AP	FPR	AUC	\overline{IoU}	\overline{F}_1	\overline{oIoU}	
SynthCP [43]	9.3	28.4	88.5	-	-	-	-
Dropout [21]	7.5	79.4	69.9	-	-	-	-
TRADI [83]	7.2	25.3	89.2	-	-	-	-
SO+H [31]	12.7	25.2	91.7	59.7	-	-	-
DML [51]	14.7	17.3	93.7	-	-	-	-
MSP [34]	7.5	27.9	90.1	65.0	46.4	35.1	29.9
ODIN [35]	7.0	28.7	90.0	65.0	41.6	28.8	36.2
ReAct [84]	10.9	21.2	92.3	62.7	46.4	34.0	28.7
SynDnsHyb	19.7	17.4	93.9	61.3	50.6	37.3	24.0
Energy [38]	12.9	18.2	93.0	63.3	50.4	42.7	29.9
OE [27]	14.6	17.7	94.0	61.7	56.1	43.8	17.9
OH [42]	19.7	56.2	88.8	66.6	-	33.9	32.7
OH*MSP [15]	18.8	30.9	89.7	66.6	-	43.6	23.0
DenseHybrid	30.2	13.0	95.6	63.0	59.7	45.8	17.2

our code base by following publicly available implementations. For the energy fine-tuning [38], we found that the optimal hyperparameters for dense setup are $m_{in} = -15$ and $m_{out} = -5$. ReAct [84] delivers the best results when the method-specific hyperparameter $c = 0.99$. Note that [39]

6.3 Ablating Components of our Hybrid Detector

Table 5 validates components of our hybrid anomaly detection approach on Fishyscapes val. The top two sections compare our hybrid anomaly detector (7) with its generative and discriminative components - $\hat{p}(\mathbf{x})$ and $P(d_{in}|\mathbf{x})$ when training on real and synthetic negative data, respectively. We observe that the hybrid detector outperforms unnormalized density which outperforms dataset posterior. We observe the same qualitative behaviour when training on real and synthetic negative data. Interestingly, the synergistic effect of compound hybrid detection is larger in the case of synthetic negatives. This finding suggests that our hybrid formulation can compensate for incomplete coverage of the out-of-distribution manifold in test images.

Bottom section replaces our unnormalized likelihood with likelihood of pre-logits as estimated by a normalizing flow. The flow is applied point-wise to obtain dense likelihood, similar to embedding density [10]. This can also be viewed as a generalization of a previous image-wide open-set approach [41] on dense predictions. We still train on negative data in an end-to-end fashion in order to make the two generative components comparable. The resulting model behaves similarly to embedding density [10] — good performance on FS Static and somewhat poorer performance on FS LostAndFound. Formulating dense likelihood

with unnormalized density (4) delivers more consistent performance than a point-wise normalizing flow on top of latent representation.

TABLE 5

Validation of hybrid anomaly detection on Fishyscapes val. Hybrid anomaly detection outperforms its generative and discriminative components. This behaviour is consistent in models trained on real and synthetic negative data, as well as for different generative components.

Anomaly detector	Neg. data	FS L&F		FS Static	
		AP	FPR	AP	FPR
Disc. $(1 - P(d_{in} \mathbf{x}))$	Real	46.5	38.3	53.5	30.9
Gen. $\hat{p}(\mathbf{x})$		58.2	7.3	58.0	5.3
Hyb. $(1 - P(d_{in} \mathbf{x}))/\hat{p}(\mathbf{x})$		60.5	6.0	63.1	4.2
Disc. $(1 - P(d_{in} \mathbf{x}))$	Syn.	30.9	61.0	29.4	71.5
Gen. $\hat{p}(\mathbf{x})$		52.8	13.1	35.8	11.1
Hyb. $(1 - P(d_{in} \mathbf{x}))/\hat{p}(\mathbf{x})$		59.5	10.4	49.0	10.3
Gen. $p(\mathbf{z})$	Real	5.7	58.9	61.7	7.6
Hyb. $(1 - P(d_{in} \mathbf{x}))/p(\mathbf{z})$		6.5	46.1	65.1	6.5

6.4 Impact of the Depth to the Detection Performance

Road driving scenes typically involve a wide range of depth. Hence, we explore the anomaly detection performance at different ranges from the camera in order to gain a better insight into the performance of different methods. We perform these experiments on LostAndFound test [12] since it allows us to compute the depth in each ground pixel. Due to errors in the provided disparity maps, we perform our analysis up to 50 meters from the camera. Table 6 indicates that DenseHybrid achieves accurate results even at large distances from the vehicle. We observe that SynBoost [18] is better than our approach at the shortest range. However, the computational complexity of image resynthesis precludes real-time deployment of such approaches [17], [18], [43] on present hardware as we show next.

TABLE 6

Anomaly detection performance at different distances from camera.

Range	MSP [34]		ML [71]		SynBoost [18]		DH (ours)	
	AP	FPR	AP	FPR	AP	FPR	AP	FPR
5-10	28.7	16.4	76.1	5.4	93.7	0.2	90.7	0.3
10-15	28.8	29.7	73.9	16.2	78.7	17.7	89.8	1.1
15-20	26.0	28.8	78.2	5.9	76.9	25.0	92.9	0.6
20-25	25.1	44.2	69.6	12.8	70.0	23.3	89.1	1.4
25-30	29.0	41.3	72.6	9.5	65.6	18.8	89.5	1.4
30-35	26.2	47.8	70.2	10.0	58.5	27.4	87.7	2.5
35-40	29.6	44.7	71.0	9.8	59.8	25.4	85.0	3.7
40-45	31.7	43.2	74.0	9.8	60.0	25.8	85.6	4.7
45-50	33.7	45.3	73.9	11.0	53.3	29.9	82.1	6.3

6.5 Inference speed

Table 7 compares computational overheads of prominent anomaly detectors on two-megapixel images. All measurements are averaged over 200 runs on RTX3090. DenseHybrid involves a negligible computational overhead of 0.1 GFLOPs and 2.8ms. These experiments indicate that image resynthesis is not applicable for real-time inference on present hardware.

TABLE 7

Computational overhead of prominent anomaly detectors over the baseline semantic segmentation model when inferring on two-megapixel images. The inference time is in milliseconds.

Method	Resynth.	Inf. time	FPS	GFLOPs
SynBoost [18]	✓	1055.5	<1	-
SynthCP [43]	✓	146.9	<1	4551.1
LDN-121 [75]	✗	60.9	16.4	202.3
LDN-121 + SML [73]	✗	75.4	13.3	202.6
LDN-121 + DH (ours)	✗	63.7	15.7	202.4

7 CONCLUSION

Discriminative and generative approaches to anomaly detection assume different failure modes. We propose to achieve synergy between these two approaches by fusing the dataset posterior with unnormalized data likelihood. We refer to the resulting method as DenseHybrid since its low computational overhead and translational equivariance are especially well suited for dense prediction context. DenseHybrid eschews the evaluation of the intractable normalization constant by leveraging negative training data. It can be trained either on real negative data sourced from some general-purpose dataset, or on synthetic negative data generated by a jointly trained normalizing flow. Finally, it can be easily attached to any closed-set segmentation approach in order to attain open-set competence. DenseHybrid yields competitive performance on the standard benchmarks for dense anomaly detection and open-set segmentation. We evaluate open-set segmentation performance according to a novel open-mIoU metric that quantifies the performance gap between closed-set and open-set conditions. Ablation experiments confirm the contributions of both components of hybrid anomaly detection. Suitable directions for future work include extending DenseHybrid towards open-set panoptics as well as towards further reduction of the performance gap between the closed-set and open-set setups.

8 LIMITATIONS

It may seem that our method may generate samples due to likelihood evaluation being a standard feature of generative models (except GANs). However, sample generation with unnormalized distributions requires MCMC sampling which can not be performed at large resolutions and dense loss, at least not with known techniques. Still, our hybrid open-set model delivers competitive performance even without the ability to generate samples. Also, variety and quality of synthetic samples are limited by the capacity of the generative model, which will be mitigated with advances in GPU design.

ACKNOWLEDGMENTS

This work has been supported by Croatian Science Foundation grant IP-2020-02-5851 ADEPT, by NVIDIA Academic Hardware Grant Program, as well as by European Regional Development Fund grants KK.01.1.1.01.0009 DATACROSS and KK.01.2.1.02.0119 A-Unit.

REFERENCES

- [1] K. He, X. Zhang, S. Ren, and J. Sun, "Deep residual learning for image recognition," in *2016 IEEE Conference on Computer Vision and Pattern Recognition, CVPR 2016*, 2016, pp. 770–778.
- [2] Z. Liu, Y. Lin, Y. Cao, H. Hu, Y. Wei, Z. Zhang, S. Lin, and B. Guo, "Swin transformer: Hierarchical vision transformer using shifted windows," in *2021 IEEE/CVF International Conference on Computer Vision, ICCV 2021*. IEEE, 2021, pp. 9992–10002.
- [3] M. Everingham, L. V. Gool, C. K. I. Williams, J. M. Winn, and A. Zisserman, "The pascal visual object classes (VOC) challenge," *Int. J. Comput. Vis.*, vol. 88, no. 2, pp. 303–338, 2010.
- [4] C. Farabet, C. Couprie, L. Najman, and Y. LeCun, "Learning hierarchical features for scene labeling," *IEEE Trans. Pattern Anal. Mach. Intell.*, vol. 35, no. 8, pp. 1915–1929, 2013.
- [5] S. Minaee, Y. Boykov, F. Porikli, A. Plaza, N. Kehtarnavaz, and D. Terzopoulos, "Image segmentation using deep learning: A survey," *IEEE Trans. Pattern Anal. Mach. Intell.*, vol. 44, no. 7, 2022.
- [6] J. R. R. Uijlings, T. Mensink, and V. Ferrari, "The missing link: Finding label relations across datasets," in *Computer Vision - ECCV 2022 - 17th European Conference*, ser. Lecture Notes in Computer Science. Springer, 2022, pp. 540–556.
- [7] X. Li, A. You, Z. Zhu, H. Zhao, M. Yang, K. Yang, S. Tan, and Y. Tong, "Semantic flow for fast and accurate scene parsing," in *Computer Vision - ECCV 2020 - 16th European Conference*, ser. Lecture Notes in Computer Science. Springer, 2020, pp. 775–793.
- [8] M. Orsic and S. Segvic, "Efficient semantic segmentation with pyramidal fusion," *Pattern Recognit.*, vol. 110, p. 107611, 2021.
- [9] H. Pan, Y. Hong, W. Sun, and Y. Jia, "Deep dual-resolution networks for real-time and accurate semantic segmentation of traffic scenes," *IEEE Trans. on Intelligent Transportation Systems*, 2022.
- [10] H. Blum, P.-E. Sarlin, J. Nieto, R. Siegwart, and C. Cadena, "The fishyscapes benchmark: Measuring blind spots in semantic segmentation," *International Journal of Computer Vision*, vol. 129, 2021.
- [11] C. González, G. Gotkowski, M. Fuchs, A. Bucher, A. Dadras, R. Fischbach, I. J. Kaltenborn, and A. Mukhopadhyay, "Distance-based detection of out-of-distribution silent failures for covid-19 lung lesion segmentation," *Medical Image Anal.*, vol. 82, 2022.
- [12] P. Pinggera, S. Ramos, S. Gehrig, U. Franke, C. Rother, and R. Mester, "Lost and found: detecting small road hazards for self-driving vehicles," in *International Conference on Intelligent Robots and Systems, IROS*, 2016.
- [13] L. Ruff, J. R. Kauffmann, R. A. Vandermeulen, G. Montavon, W. Samek, M. Kloft, T. G. Dietterich, and K. Müller, "A unifying review of deep and shallow anomaly detection," *Proc. IEEE*, vol. 109, no. 5, pp. 756–795, 2021.
- [14] T. E. Boult, S. Cruz, A. R. Dhamija, M. Günther, J. Henrydoss, and W. J. Scheirer, "Learning and the unknown: Surveying steps toward open world recognition," in *AAAI Conference on Artificial Intelligence*. AAAI Press, 2019.
- [15] P. Bevandić, I. Krešo, M. Oršić, and S. Šegvić, "Dense open-set recognition based on training with noisy negative images," *Image and Vision Computing*, vol. 124, p. 104490, 2022.
- [16] H. Blum, P. Sarlin, J. I. Nieto, R. Siegwart, and C. Cadena, "Fishyscapes: A benchmark for safe semantic segmentation in autonomous driving," in *2019 IEEE/CVF International Conference on Computer Vision Workshops*. IEEE, 2019, pp. 2403–2412.
- [17] K. Lis, K. K. Nakka, P. Fua, and M. Salzmann, "Detecting the unexpected via image resynthesis," in *International Conference on Computer Vision, ICCV*, 2019.
- [18] G. D. Biase, H. Blum, R. Siegwart, and C. Cadena, "Pixel-wise anomaly detection in complex driving scenes," in *Computer Vision and Pattern Recognition, CVPR*, 2021.
- [19] T. Vojir, T. Šipka, R. Aljundi, N. Chumerin, D. O. Reino, and J. Matas, "Road anomaly detection by partial image reconstruction with segmentation coupling," in *International Conference on Computer Vision, ICCV*, 2021.
- [20] T. DeVries and G. W. Taylor, "Learning confidence for out-of-distribution detection in neural networks," *CoRR*, vol. abs/1802.04865, 2018.
- [21] A. Kendall and Y. Gal, "What uncertainties do we need in bayesian deep learning for computer vision?" in *Neural Information Processing Systems*, 2017.
- [22] E. T. Nalisnick, A. Matsukawa, Y. W. Teh, D. Görür, and B. Lakshminarayanan, "Do deep generative models know what they don't know?" in *7th International Conference on Learning Representations, ICLR*, 2019.
- [23] J. Serrà, D. Álvarez, V. Gómez, O. Slizovskaia, J. F. Núñez, and J. Luque, "Input complexity and out-of-distribution detection with likelihood-based generative models," in *8th International Conference on Learning Representations, ICLR*, 2020.
- [24] T. Lucas, K. Shmelkov, K. Alahari, C. Schmid, and J. Verbeek, "Adaptive density estimation for generative models," in *Neural Information Processing Systems*, 2019.
- [25] L. H. Zhang, M. Goldstein, and R. Ranganath, "Understanding failures in out-of-distribution detection with deep generative models," in *International Conference on Machine Learning, ICML*, 2021.
- [26] R. Chan, M. Rottmann, and H. Gottschalk, "Entropy maximization and meta classification for out-of-distribution detection in semantic segmentation," in *International Conference on Computer Vision, ICCV*, 2021.
- [27] D. Hendrycks, M. Mazeika, and T. G. Dietterich, "Deep anomaly detection with outlier exposure," in *7th International Conference on Learning Representations, ICLR*, 2019.
- [28] K. Lee, H. Lee, K. Lee, and J. Shin, "Training confidence-calibrated classifiers for detecting out-of-distribution samples," in *6th International Conference on Learning Representations, ICLR*, 2018.
- [29] L. Neal, M. L. Olson, X. Z. Fern, W. Wong, and F. Li, "Open set learning with counterfactual images," in *ECCV 2018 - 15th European Conference, Munich, German*, 2018.
- [30] Z. Zhao, L. Cao, and K. Lin, "Revealing distributional vulnerability of explicit discriminators by implicit generators," *CoRR*, vol. abs/2108.09976, 2021.
- [31] M. Grcić, P. Bevandić, and S. Šegvić, "Dense open-set recognition with synthetic outliers generated by real NVP," in *16th International Joint Conference on Computer Vision, Imaging and Computer Graphics Theory and Applications, VISIGRAPP*, 2021.
- [32] M. Grcic, P. Bevandic, and S. Segvic, "Densehybrid: Hybrid anomaly detection for dense open-set recognition," in *European Conference on Computer Vision, ECCV 2022*. Springer, 2022.
- [33] D. M. Hawkins, *Identification of Outliers*, ser. Monographs on Applied Probability and Statistics. Springer, 1980.
- [34] D. Hendrycks and K. Gimpel, "A baseline for detecting misclassified and out-of-distribution examples in neural networks," in *5th International Conference on Learning Representations, ICLR*, 2017.
- [35] S. Liang, Y. Li, and R. Srikant, "Enhancing the reliability of out-of-distribution image detection in neural networks," in *6th International Conference on Learning Representations, ICLR*, 2018.
- [36] B. Lakshminarayanan, A. Pritzel, and C. Blundell, "Simple and scalable predictive uncertainty estimation using deep ensembles," in *Advances in Neural Information Processing Systems 30: Annual Conference on Neural Information Processing Systems*, 2017.
- [37] A. R. Dhamija, M. Günther, and T. E. Boult, "Reducing network agnostophobia," in *Annual Conference on Neural Information Processing Systems 2018, NeurIPS*, 2018.
- [38] W. Liu, X. Wang, J. D. Owens, and Y. Li, "Energy-based out-of-distribution detection," in *NeurIPS*, 2020.
- [39] V. Besnier, A. Bursuc, D. Picard, and A. Briot, "Triggering failures: Out-of-distribution detection by learning from local adversarial attacks in semantic segmentation," in *2021 IEEE/CVF International Conference on Computer Vision, ICCV 2021*, 2021.
- [40] S. Kong and D. Ramanan, "Opengan: Open-set recognition via open data generation," *IEEE Transactions on Pattern Analysis and Machine Intelligence*, 2022.
- [41] H. Zhang, A. Li, J. Guo, and Y. Guo, "Hybrid models for open set recognition," in *European Conference on Computer Vision ECCV*, 2020.
- [42] P. Bevandic, I. Kreso, M. Orsic, and S. Segvic, "Simultaneous semantic segmentation and outlier detection in presence of domain shift," in *41st DAGM German Conference, DAGM GCP, 2019*.
- [43] Y. Xia, Y. Zhang, F. Liu, W. Shen, and A. L. Yuille, "Synthesize then compare: Detecting failures and anomalies for semantic segmentation," in *European Conference on Computer Vision, ECCV*, 2020.
- [44] V. Zavrtnik, M. Kristan, and D. Skocaj, "Reconstruction by inpainting for visual anomaly detection," *Pattern Recognit.*, vol. 112, p. 107706, 2021.
- [45] W. Grathwohl, K. Wang, J. Jacobsen, D. Duvenaud, M. Norouzi, and K. Swersky, "Your classifier is secretly an energy based model and you should treat it like one," in *8th International Conference on Learning Representations, ICLR 2020*, 2020.
- [46] Y. Tian, Y. Liu, G. Pang, F. Liu, Y. Chen, and G. Carneiro, "Pixel-wise energy-biased abstention learning for anomaly segmentation on complex urban driving scenes," in *Computer Vision - ECCV 2022 - 17th European Conference*. Springer, 2022.

- [47] C. Liang, W. Wang, J. Miao, and Y. Yang, "Gmmseg: Gaussian mixture based generative semantic segmentation models," *Advances in Neural Information Processing Systems*, 2022.
- [48] W. J. Scheirer, A. de Rezende Rocha, A. Sapkota, and T. E. Boulton, "Toward open set recognition," *IEEE Transactions on Pattern Analysis and Machine Intelligence*, vol. 35, no. 7, pp. 1757–1772, 2013.
- [49] W. J. Scheirer, L. P. Jain, and T. E. Boulton, "Probability models for open set recognition," *IEEE Trans. Pattern Anal. Mach. Intell.*, vol. 36, no. 11, pp. 2317–2324, 2014.
- [50] A. Bendale and T. E. Boulton, "Towards open set deep networks," in *IEEE Conference on Computer Vision and Pattern Recognition, CVPR*, 2016.
- [51] J. Cen, P. Yun, J. Cai, M. Y. Wang, and M. Liu, "Deep metric learning for open world semantic segmentation," in *Proceedings of the IEEE/CVF International Conference on Computer Vision (ICCV)*, October 2021, pp. 15333–15342.
- [52] S. Vaze, K. Han, A. Vedaldi, and A. Zisserman, "Open-set recognition: A good closed-set classifier is all you need," in *The Tenth International Conference on Learning Representations, ICLR 2022*, 2022.
- [53] G. Chen, P. Peng, X. Wang, and Y. Tian, "Adversarial reciprocal points learning for open set recognition," *IEEE Trans. Pattern Anal. Mach. Intell.*, 2022.
- [54] C. Geng, S. Huang, and S. Chen, "Recent advances in open set recognition: A survey," *IEEE Trans. Pattern Anal. Mach. Intell.*, vol. 43, no. 10, pp. 3614–3631, 2021.
- [55] O. Zendel, K. Honauer, M. Murschitz, D. Steininger, and G. F. Dominguez, "Wilddash - creating hazard-aware benchmarks," in *European Conference on Computer Vision (ECCV)*, 2018.
- [56] R. Chan, K. Lis, S. Uhlemeyer, H. Blum, S. Honari, R. Siegwart, P. Fua, M. Salzmann, and M. Rottmann, "Segmentmeifyoucan: A benchmark for anomaly segmentation," in *Proceedings of the Neural Information Processing Systems Track on Datasets and Benchmarks 1, NeurIPS Datasets and Benchmarks 2021*, 2021.
- [57] M. Sokolova and G. Lapalme, "A systematic analysis of performance measures for classification tasks," *Inf. Process. Manag.*, vol. 45, no. 4, pp. 427–437, 2009.
- [58] M. D. Scherrek and B. D. Rigling, "Open set recognition for automatic target classification with rejection," *IEEE Trans. Aerosp. Electron. Syst.*, vol. 52, no. 2, pp. 632–642, 2016.
- [59] C. Sakaridis, D. Dai, and L. V. Gool, "Map-guided curriculum domain adaptation and uncertainty-aware evaluation for semantic nighttime image segmentation," *IEEE Trans. Pattern Anal. Mach. Intell.*, vol. 44, no. 6, 2022.
- [60] X. Du, Z. Wang, M. Cai, and Y. Li, "VOS: learning what you don't know by virtual outlier synthesis," in *The Tenth International Conference on Learning Representations, ICLR 2022*, 2022.
- [61] U. Michieli and P. Zanuttigh, "Knowledge distillation for incremental learning in semantic segmentation," *Comput. Vis. Image Underst.*, vol. 205, p. 103167, 2021.
- [62] S. Uhlemeyer, M. Rottmann, and H. Gottschalk, "Towards unsupervised open world semantic segmentation," in *The 38th Conference on Uncertainty in Artificial Intelligence*, 2022.
- [63] Y. Fu, X. Wang, H. Dong, Y. Jiang, M. Wang, X. Xue, and L. Sigal, "Vocabulary-informed zero-shot and open-set learning," *IEEE Trans. Pattern Anal. Mach. Intell.*, vol. 42, no. 12, 2020.
- [64] Y. Xian, C. H. Lampert, B. Schiele, and Z. Akata, "Zero-shot learning - A comprehensive evaluation of the good, the bad and the ugly," *IEEE Trans. Pattern Anal. Mach. Intell.*, vol. 41, no. 9, pp. 2251–2265, 2019.
- [65] T. Salimans, I. J. Goodfellow, W. Zaremba, V. Cheung, A. Radford, and X. Chen, "Improved techniques for training gans," in *Neural Information Processing Systems 2016*, 2016, pp. 2226–2234.
- [66] Y. Du and I. Mordatch, "Implicit generation and modeling with energy based models," in *Neural Information Processing Systems 2019, NeurIPS 2019*, 2019.
- [67] Y. Song and S. Ermon, "Generative modeling by estimating gradients of the data distribution," in *Neural Information Processing Systems 2019, NeurIPS 2019*, 2019, pp. 11895–11907.
- [68] S. Kong and D. Ramanan, "An empirical exploration of open-set recognition via lightweight statistical pipelines," 2021. [Online]. Available: <https://openreview.net/forum?id=0Zxk3ynq7JE>
- [69] M. Grcić, I. Grubišić, and S. Šegvić, "Densely connected normalizing flows," in *Neural Information Processing Systems*, 2021.
- [70] M. Grcić, I. Grubišić, and S. Šegvić, "Densely connected normalizing flows," *CoRR*, vol. abs/2106.04627, 2021.
- [71] D. Hendrycks, S. Basart, M. Mazeika, A. Zou, J. Kwon, M. Mostajabi, J. Steinhardt, and D. Song, "Scaling out-of-distribution detection for real-world settings," in *International Conference on Machine Learning, ICML*, 2022.
- [72] K. Lis, S. Honari, P. Fua, and M. Salzmann, "Detecting road obstacles by erasing them," *CoRR*, vol. abs/2012.13633, 2020.
- [73] S. Jung, J. Lee, D. Gwak, S. Choi, and J. Choo, "Standardized max logits: A simple yet effective approach for identifying unexpected road obstacles in urban-scene segmentation," in *International Conference on Computer Vision, ICCV*, 2021.
- [74] A. Malinin and M. J. F. Gales, "Predictive uncertainty estimation via prior networks," in *Annual Conference on Neural Information Processing Systems*, 2018.
- [75] I. Kreso, J. Krapac, and S. Segvic, "Efficient ladder-style densenets for semantic segmentation of large images," *IEEE Trans. Intell. Transp. Syst.*, vol. 22, 2021.
- [76] M. Cordts, M. Omran, S. Ramos, T. Rehfeld, M. Enzweiler, R. Benenson, U. Franke, S. Roth, and B. Schiele, "The cityscapes dataset for semantic urban scene understanding," in *IEEE Conference on Computer Vision and Pattern Recognition, CVPR*, 2016.
- [77] G. Neuhold, T. Ollmann, S. R. Bulò, and P. Kotschieder, "The mapillary vistas dataset for semantic understanding of street scenes," in *IEEE International Conference on Computer Vision, ICCV*, 2017.
- [78] Y. Zhu, K. Sapra, F. A. Reda, K. J. Shih, S. D. Newsam, A. Tao, and B. Catanzaro, "Improving semantic segmentation via video propagation and label relaxation," in *IEEE Conference on Computer Vision and Pattern Recognition, CVPR 2019*, 2019.
- [79] M. Grcić, "Densehybrid source code: <https://github.com/matejgrcic/DenseHybrid>," 2022.
- [80] P. Oza and V. M. Patel, "C2ae: Class conditioned auto-encoder for open-set recognition," in *Proceedings of the IEEE/CVF Conference on Computer Vision and Pattern Recognition (CVPR)*, June 2019.
- [81] K. Lee, K. Lee, H. Lee, and J. Shin, "A simple unified framework for detecting out-of-distribution samples and adversarial attacks," in *Neural Information Processing Systems, NeurIPS*, 2018.
- [82] J. Steinhardt and P. Liang, "Unsupervised risk estimation using only conditional independence structure," in *Neural Information Processing Systems 2016*, 2016, pp. 3657–3665.
- [83] G. Franchi, A. Bursuc, E. Aldea, S. Dubuisson, and I. Bloch, "TRADI: tracking deep neural network weight distributions," in *16th European Conference on Computer Vision, ECCV*, 2020.
- [84] Y. Sun, C. Guo, and Y. Li, "React: Out-of-distribution detection with rectified activations," in *NeurIPS*, 2021.



Matej Grcić received a M.Sc. degree from the Faculty of Electrical Engineering and Computing in Zagreb. He finished the master study program in Computer Science in 2020. He is pursuing his Ph.D. degree at University of Zagreb, FER. His research interests include generative modeling and open-world recognition.



Siniša Šegvić received a Ph.D. degree in computer science from the University of Zagreb, Croatia. He was a post-doctoral researcher at IRISA Rennes and also at TU Graz. He is currently a full professor at Uni-ZG FER. His research interests focus on deep convolutional architectures for classification and dense prediction.